Обзор ArXiv: astro-ph
23-28 февраля 2018 года

От Сильченко О.К.

Astro-ph: 1802.09453

BARYON BUDGET OF THE HOT CIRCUMGALACTIC MEDIUM OF MASSIVE SPIRAL GALAXIES

Jiang-Tao Li[1], Joel N. Bregman[1], Q. Daniel Wang[2], Robert A. Crain[3], and Michael E. Anderson[4]

Draft version February 27, 2018

ABSTRACT

The baryon content around local galaxies is observed to be much less than is needed in Big Bang nucleosynthesis. Simulations indicate that a significant fraction of these "missing baryons" may be stored in a hot tenuous circum-galactic medium (CGM) around massive galaxies extending to or even beyond the virial radius of their dark matter halos. Previous observations in X-ray and Sunyaev-Zel'dovich (SZ) signal claimed that $\sim (1-50)\%$ of the expected baryons are stored in a hot CGM within the virial radius. The large scatter is mainly caused by the very uncertain extrapolation of the hot gas density profile based on the detection in a small radial range (typically within 10%-20% of the virial radius). Here we report stacking X-ray observations of six local isolated massive spiral galaxies from the CGM-MASS sample. We find that the mean density profile can be characterized by a single power law out to a galactocentric radius of ≈ 200 kpc (or ≈ 130 kpc above the 1 σ background uncertainty), about half the virial radius of the dark matter halo. We can now estimate that the hot CGM within the virial radius accounts for $(8 \pm 4)\%$ of the baryonic mass expected for the halos. Including the stars, the baryon fraction is $(27 \pm 16)\%$, or $(39 \pm 20)\%$ by assuming a flattened density profile at $r \gtrsim 130$ kpc. We conclude that the hot baryons within the virial radius of massive galaxy halos are insufficient to explain the "missing baryons".

Выборка

We studied the hot gaseous halo of six isolated spiral galaxies, which are among the most massive in the local universe ($d < 100$ Mpc), with a stellar mass $M_* \gtrsim 1.5 \times 10^{11}$ $M_\odot$ and rotation velocity $v_{rot} > 300$ km s^{-1}. This study is based on the analysis of the observations from a large *XMM-Newton* program conducted in AO-

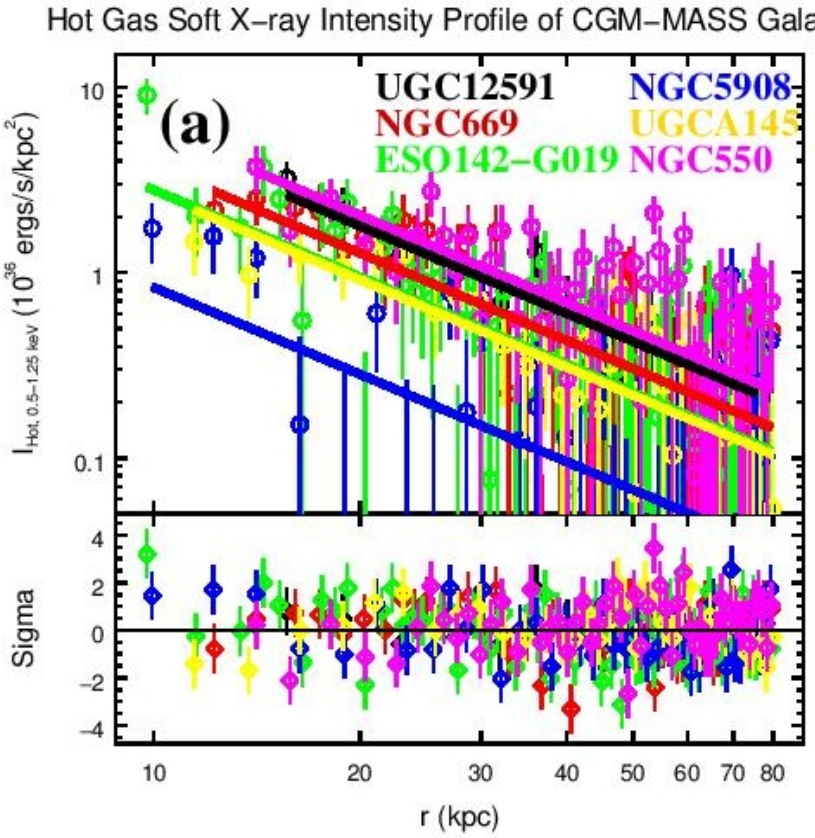
Hot Gas Soft X−ray Intensity Profile of CGM−MASS Galaxies
(a)
UGC12591
NGC5908
NGC669
UGCA145
ESO142−G019
NGC550
$I_{Hot,\ 0.5-1.25\ keV}$ (10^{36} ergs/s/kpc^2)
Sigma
r (kpc)

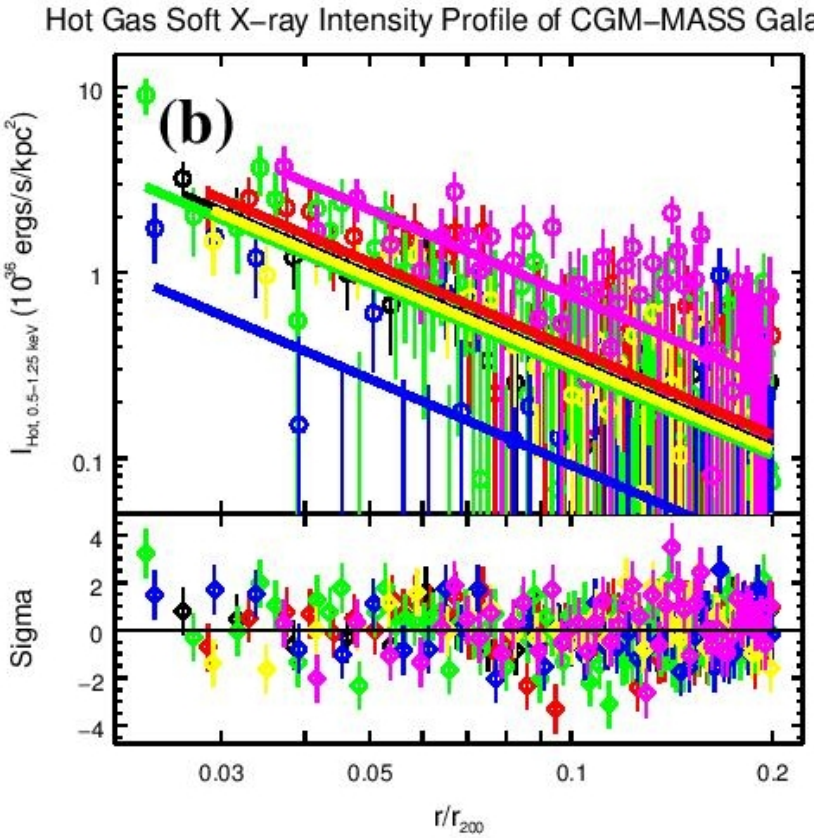
Hot Gas Soft X−ray Intensity Profile of CGM−MASS Galaxies
(b)
$I_{Hot,\ 0.5-1.25\ keV}$ (10^{36} ergs/s/kpc^2)
Sigma
r/r_{200}

Все сложили

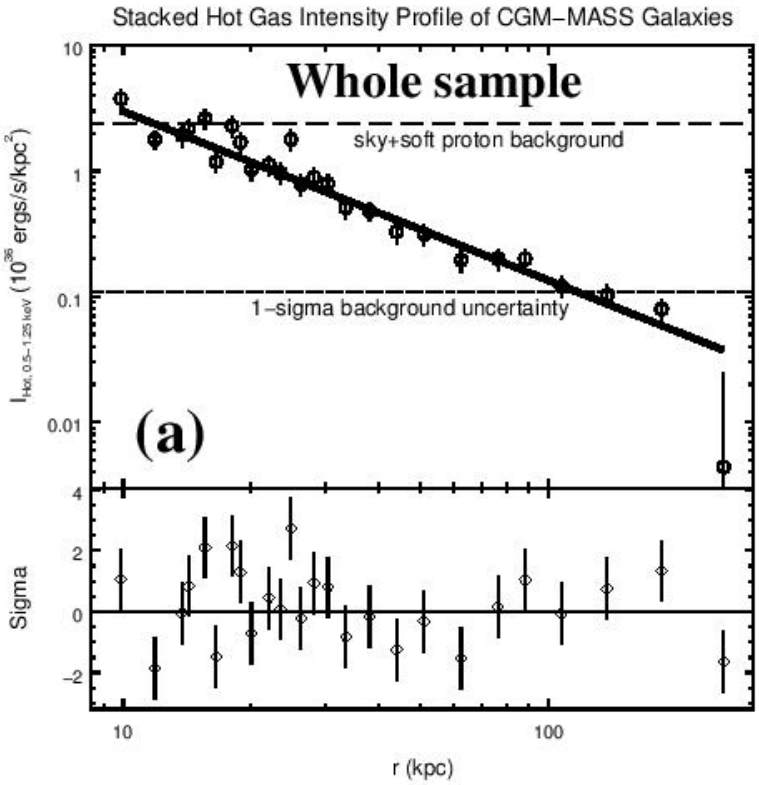

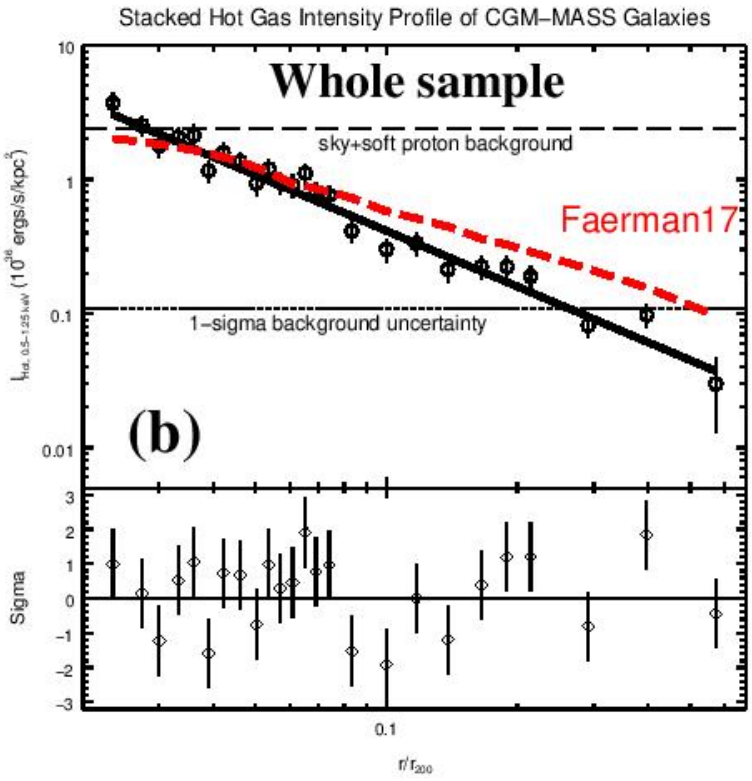

Наклон постоянный!

Выводы

The cosmic baryon fraction, or the baryon-to-total (baryon+dark matter) mass ratio, is $(16.69 \pm 0.63)\%$ (Komatsu et al. 2009). By extrapolating the X-ray intensity profile to r_{200}, the derived mass of the hot CGM accounts for $(7.8 \pm 3.6)\%$ of the expected baryons. Assuming the mass of other cooler gas phases are negligible for such massive quiescent galaxies (e.g., Li et al. 2016), the total (stellar+hot gas) baryons detected within r_{200} accounts for $(27 \pm 16)\%$ of the expected baryons, implying that $\sim 73\%$ of the baryons are still "missing" from the current survey of baryons in stars and the hot CGM. Compared to the $L^\star$ galaxy studied by the COS-Halos group, which has only $< 6\%$ of the baryons stored in the extended hot CGM (Werk et al. 2014), our fiducial galaxy has $\sim 29\%$ of the baryons in hot phase, or the total mass of the extended hot halo is $\sim 45\%$ of the stellar mass of the galaxy within r_{200}.

Сравнение в интервале масс

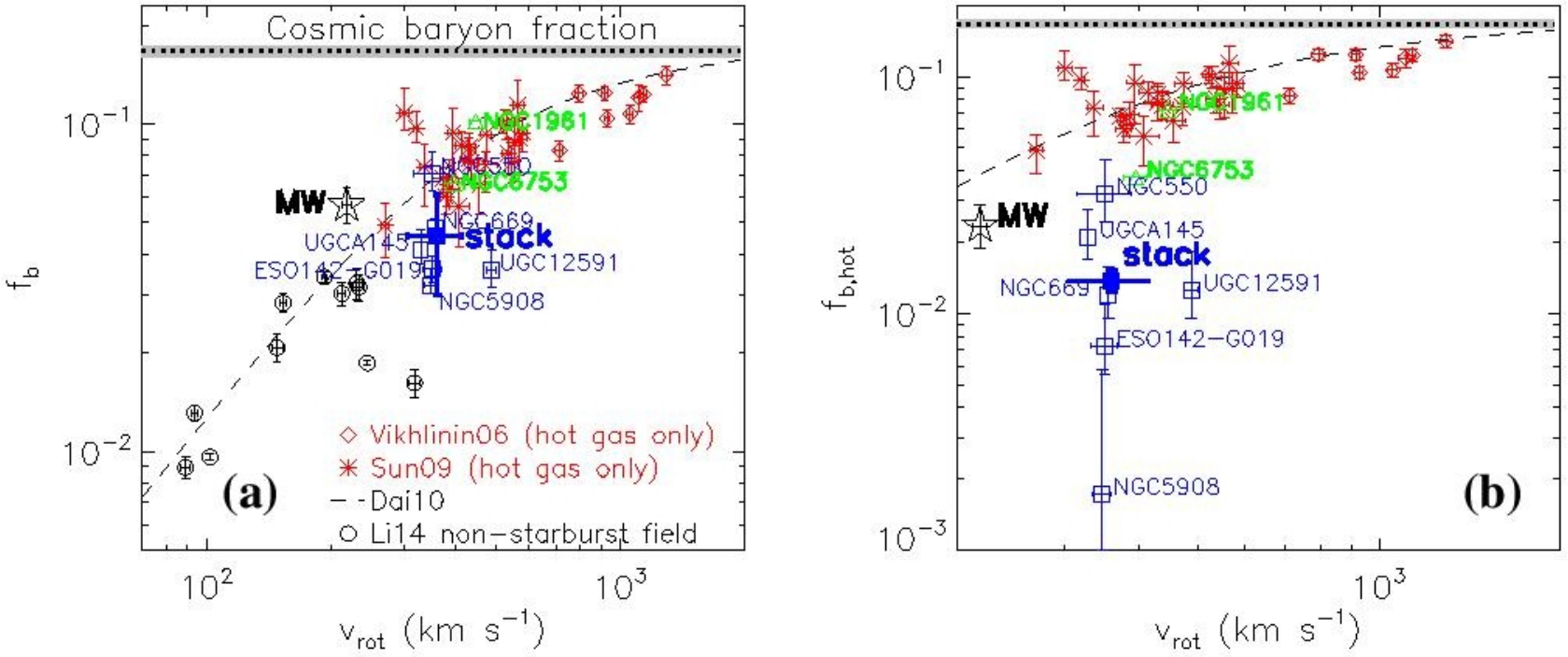

FIG. 4.— **(a)** Baryon fraction (f_b) v.s. rotation velocity (v_{rot}). The cosmic baryon fraction (dotted line) with error (shaded area), a fitted relation from Dai et al. (2010) (dashed), the MW (Miller & Bregman 2015) (black five-pointed star), samples of non-starburst field spirals (Li et al. 2014) (black circles), galaxy groups (Sun et al. 2009) (red stars), and galaxy clusters (Vikhlinin et al. 2006) (red diamonds) are plotted for comparison. For the non-starburst field spirals, only the stellar mass and the hot gas within a few tens of kpc are included in the baryon budget; an extended hot halo is not detected. For galaxy groups and clusters, only the hot gas component (no stellar component) is included, and we have simply assumed the rotation velocity equals to the velocity dispersion for a qualitative comparison. **(b)** Hot gas baryon fraction ($f_{b,hot}$) v.s. v_{rot}. We include only the extended hot gas component for a uniform comparison, with no stellar component

Astro-ph: 1802.09495

The Diversity of Atomic Hydrogen in Slow Rotator Early-type Galaxies

Lisa M. Young,[1,2]★ Paolo Serra,[3] Davor Krajnović,[4] and Pierre-Alain Duc[5]
[1] *Physics Department, New Mexico Tech, 801 Leroy Place, Socorro, NM 87801 USA*
[2] *Adjunct Astronomer, National Radio Astronomy Observatory*
[3] *INAF - Osservatorio Astronomico di Cagliari, Via della Scienza 5, I-09047 Selargius (CA), Italy*
[4] *Leibniz-Institut für Astrophysik Potsdam (AIP), An der Sternwarte 16, D-14482 Potsdam, Germany*
[5] *Observatoire Astronomique de Strasbourg, Université de Strasbourg, CNRS, UMR 7550, 11 rue de l'Université, F-67000 Strasbourg, France*

Accepted XXX. Received YYY; in original form ZZZ

ABSTRACT

We present interferometric observations of H I in nine slow rotator early-type galaxies of the ATLAS^{3D} sample. With these data, we now have sensitive H I searches in 34 of the 36 slow rotators. The aggregate detection rate is 32% ± 8%, consistent with previous work; however, we find two detections with extremely high H I masses, whose gas kinematics are substantially different from what was previously known about H I in slow rotators. These two cases (NGC 1222 and NGC 4191) broaden the known diversity of H I properties in slow rotators. NGC 1222 is a merger remnant with prolate-like

Выборка

Table 2. H I image properties for Atlas3D galaxies.

Type	Target	Dist. (Mpc)	Vel. range (km s^{-1})	beam (″)	beam (kpc)	Δv (km s^{-1})	rms (mJy/bm)	N(H I) lim (10^{19} cm^{-2})	S(H I) (Jy km s^{-1})	M(H I) ($M_\odot$)
(1)	(2)	(3)	(4)	(5)	(6)	(7)	(8)	(9)	(10)	(11)
	NGC 1222	33.3	1865 – 3060	20 × 15	3.2 × 2.4	21.0	1.15	43	11.2±0.7	$(2.9\pm0.2)\times10^9$
	NGC 1289	38.4	2206 – 3466	77 × 50	14 × 9.3	42.0	0.40	2.4	< 0.13	$< 4.7\times10^7$
	NGC 4191	39.2	1132 – 4172	49 × 45	9.3 × 8.6	16.0	0.70	2.7	10.1±0.3	$(3.7\pm0.1)\times10^9$
	NGC 4636	14.3	143 – 1663	51 × 45	3.5 × 3.1	16.0	0.70	2.7	< 0.15	$< 7.0\times10^6$
Slow Rotators	NGC 4690	40.2	1216 – 4264	70 × 50	14 × 9.7	16.0	0.80	2.0	< 0.16	$< 6.3\times10^7$
	NGC 5576	24.8	–4 – 3020	54 × 46	6.5 × 5.5	16.0	0.65	2.3	< 0.14	$< 2.0\times10^7$
	NGC 5813	31.3	421 – 3453	51 × 46	7.7 × 7.0	16.0	0.67	2.5	< 0.14	$< 3.2\times10^7$
	NGC 5831	26.4	1324 – 2367	57 × 50	7.3 × 6.4	22.0	0.48	2.0	< 0.12	$< 1.9\times10^7$
	NGC 5846	24.2	1324 – 2367	57 × 50	6.7 × 5.8	22.0	0.48	2.0	< 0.12	$< 1.6\times10^7$
	NGC 5574	23.2	–4 – 3020	54 × 46	6.1 × 5.2	16.0	0.65	2.3	< 0.14	$< 1.7\times10^7$
Fast Rotators	NGC 5838	21.8	1324 – 2367	57 × 50	6.0 × 5.3	22.0	0.48	2.0	< 0.12	$< 1.3\times10^7$
	NGC 5845	25.2	1324 – 2367	57 × 50	7.0 × 6.1	22.0	0.48	2.0	< 0.12	$< 1.8\times10^7$

Distances are taken from Cappellari et al. (2011a). The velocity range in column 4 indicates the usable range covered by the data. Column 7 gives the channel widths in the image cubes used for analysis; for the newer data, these are significantly wider than the intrinsic resolution of the data. The column density limit represents 5σ in one channel and the integrated flux density limit represents three times the statistical uncertainty in a sum over 6 beams and 50 km s^{-1}.

Полная статистика по HI: медленные ротаторы - слева

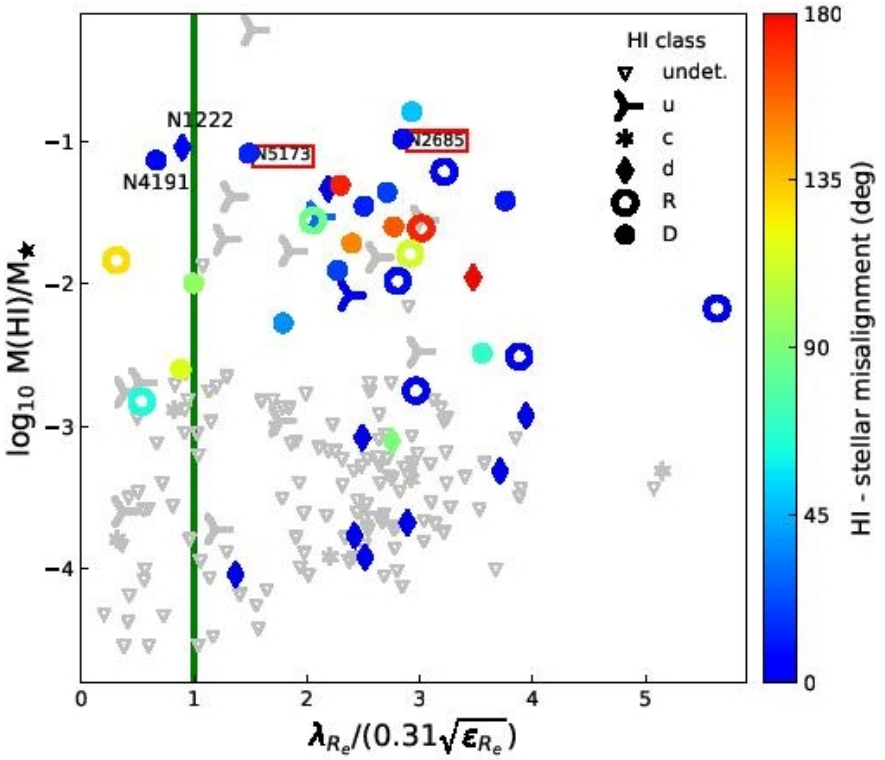

Figure 3. An updated version of Figure 5 from S14. HI masses in the ATLAS^{3D} sample are plotted against a scaled version of the stellar specific angular momentum parameter λ_{R_e}. Slow rotators are located to the left of the vertical line and fast rotators are to the right. The symbol shapes indicate the HI morphology: *u* are unsettled distributions like tails or streams, *c* are small clouds, *d* are small discs, *D* are large discs, and *R* are rings. The symbol

NGC 4191

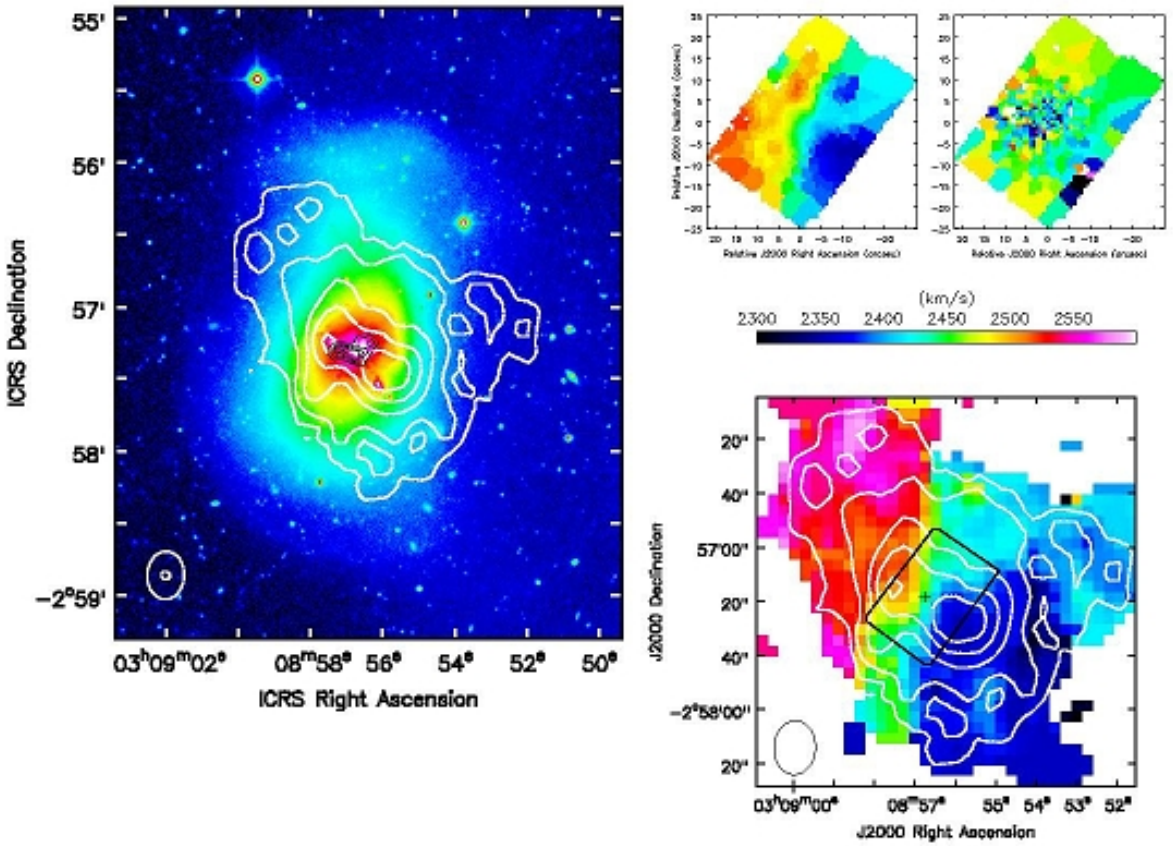

Figure 5. NGC 1222. Left: Optical is the g-band MATLAS image from Duc et al. (2015). White contours show the H I distribution; contours are (0.1, 0.2, 0.4, 0.6, 0.8) times the peak, which is 1.14 Jy beam^{-1} km s^{-1} or 4.1×10^{21} cm^{-2}. Black contours show the CO distribution from Alatalo et al. (2013); they are (0.2, 0.4, 0.6, 0.8) times the peak value of 17.5 Jy beam^{-1} km s^{-1} or 4.2×10^{22} molecules cm^{-2} at a conversion factor of 3×10^{20} molecules cm^{-2} per (K km s^{-1}). Right: Velocity fields in NGC 1222. The lower image shows H I velocities; the black cross marks the optical nucleus and the black polygon shows the field of view for the optical velocity data. The upper pair are the [O III] velocities (left) and the stellar velocities (right). All the velocity fields use the same colour scale.

NGC 1222

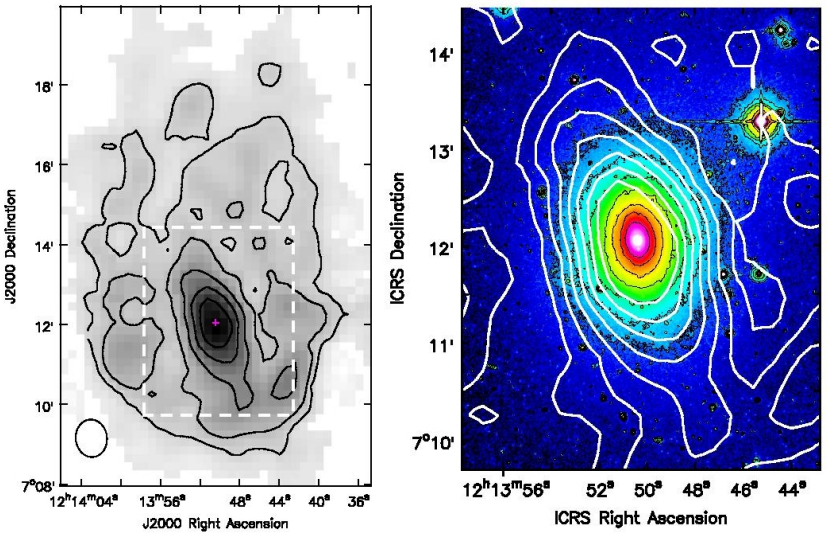
J2000 Declination
J2000 Right Ascension
ICRS Declination
ICRS Right Ascension

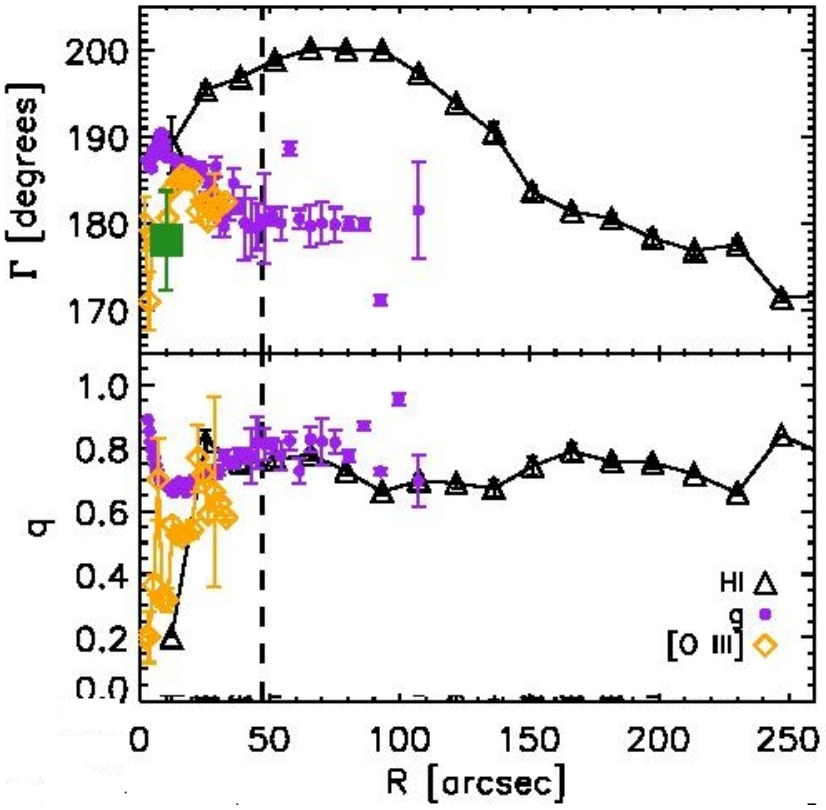
Γ [degrees]
q
R [arcsec]
HI
[O III]

Astro-ph: 1802.09540

The hELENa project – II. Abundance distribution trends of early-type galaxies: from dwarfs to giants

A. Sybilska[1,2]*, H. Kuntschner[2], G. van de Ven[3], A. Vazdekis[4,5], J. Falcón-Barroso[4,5], R. F. Peletier[6], T. Lisker[7]

[1]*Baltic Institute of Technology, al. Zwycięstwa 96/98, 81-451 Gdynia, Poland*
[2]*European Southern Observatory, Karl-Schwarzschild-Strasse 2, 85748 Garching bei München, Germany*
[3]*Max Planck Institute for Astronomy, Königstuhl 17, 69117 Heidelberg, Germany*
[4]*Instituto de Astrofísica de Canarias, Vía Láctea s/n, E-38205 La Laguna, Tenerife, Spain*
[5]*Departamento de Astrofísica, Universidad de La Laguna, E-38200 La Laguna, Tenerife, Spain*
[6]*Kapteyn Astronomical Institute, University of Groningen, Postbus 800, 9700 AV Groningen, the Netherlands*
[7]*Astronomisches Rechen-Institut, Zentrum für Astronomie der Universität Heidelberg, Mönchhofstrasse 12-14, D-69120 Heidelberg, Germany*

ABSTRACT

In this second paper of **T**he role of **E**nvironment in shaping **L**ow-mass **E**arly-type **N**earby g**a**laxies (hELENa) series we study [Mg/Fe] abundance distribution trends of early-type galaxies observed with the SAURON integral field unit, spanning a wide range in mass and local environment densities: 20 low-mass early-types (dEs) of Sybilska et al. (2017) and 258 massive early types (ETGs) of the ATLAS^{3D} project, all homogeneously reduced and ana-

Исследуемая выборка

Our low-mass early-type sample consists of 20 dwarf early-types (Sybilska et al. 2017, hereafter S17), 17 of which are located in the Virgo cluster and three in the field. The galaxies have been drawn from the high-mass end of the dE luminosity function and comprise objects of various dE subtypes (disky, blue-core, as well as nucleated and non-nucleated galaxies), as well as a range of ellipticities and locations within the Virgo cluster.

The massive early-type sample consists of 258 ATLAS^{3D} galaxies: 58 Virgo cluster and 200 field/group objects. The population parameters presented here are, as described in S17, based on the line-strength measurements of Scott et al. (2013), which were transformed from the Lick to the LIS system of Vazdekis et al. (2010) and for which stellar population estimates were then derived

Вычисление [Mg/Fe]

The methods for the derivation of [M/H] and [Mg/Fe] abundance ratios are described in Sec. 3.6 and 3.7 of S17. In short, we use the abundance-ratio insensitive index combination [MgFe50] of Kuntschner et al. (2010) as well as the optimized Hβ_o index defined by Cervantes & Vazdekis (2009) which is less dependent on metallicity than the traditional Hβ index. We then derive age and metallicity ([M/H]) with the help of MILES stellar population models of Vazdekis et al. (2015), linearly interpolating between the available model prediction. To reduce the effects of grid discretization, we oversample the original models using a linear interpolation in the age-[M/H]-[index] space. [Fe/H] values are subsequently calculated using the following formula: $[Fe/H] = [M/H]0.75 \cdot [Mg/Fe]$ (ibid.).

To derive the [Mg/Fe] abundance ratios we interpolate between the predictions of MILES scaled-solar and α-enhanced models on the Mg b-Fe5015 plane. For each line strength measurement we extracte Mg b and Fe5015 index pairs from both sets of models, corresponding to the best-fitting single stellar population (SSP) age and metallicity derived by interpolating between model predictions in the Hβ_o-[MgFe50]' plane. We then calculate the

Выборки для сравнения

Table 1. Basic details of the literature samples used in the study.

data type	source	sample info	instrument	mass (range) $[M_\odot]$
unresolved/IFU	Sybilska et al. (2017)	20 dEs, Virgo and field	SAURON/WHT	$1.68{\cdot}10^9 - 8.18{\cdot}10^9$ [a]
	Scott et al. (2013)	258 ETGs, Virgo and field	SAURON/WHT	$3.86{\cdot}10^9 - 5.96{\cdot}10^{11}$ [b]
resolved	Tolstoy et al. (2009)[g]	Sculptor	UVES/VLT	$1.3{\pm}0.3, 2.3{\pm}0.2 \cdot 10^7$ [c]
		Fornax	UVES/VLT, FLAMES/VLT	$5.3{\pm}0.6, 7.4{\pm}0.4 \cdot 10^7$ [c]
		Carina	UVES/VLT	$0.6{\pm}0.2, 1.0{\pm}0.1 \cdot 10^7$ [c]
		Sagittarius	HIRES/Keck, FLAMES/VLT, UVES/VLT	$1 \cdot 10^9$ [d]
	Kirby et al. (2011)	Sculptor	DEIMOS/Keck	$1.3{\pm}0.3, 2.3{\pm}0.2 \cdot 10^7$ [c]
		Leo I	DEIMOS/Keck	$1.2{\pm}0.3, 2.2{\pm}0.2 \cdot 10^7$ [c]
	Pompéia et al. (2008)	LMC	FLAMES/VLT	$1.7{\pm}0.7 \cdot 10^{10}$ [e]
	Bensby et al. (2014)	Milky Way	FEROS/ESO 1.5m, 2.2 m; SOFIN,FIES/NOT; UVES/VLT; HARPS/ESO 3.6 m; MIKE/Magellan Clay telescope	$1.39{\pm}0.49 \cdot 10^{12}$ [f]

[a] M_{vir} mass range based on R_e and σ values of Sybilska et al. (2017); [b] M_{JAM} mass range from Cappellari et al. (2013); [c] $M_{1/2}$ from Collins et al. (2014) and Wolf et al. (2010), respectively; [d] Total mass of the best fitting cuspy/core model from Majewski et al. (2013); [e] M(8.7 kpc) from van der Marel & Kallivayalil (2014); [f] M_{100} mass of Watkins et al. (2010); [g] compiled from Shetrone et al. (2003), Geisler et al. (2005), McWilliam & Smecker-Hane (2005), Letarte (2007), Sbordone et al. (2007), and Koch et al. (2008).

Индивидуальные галактики

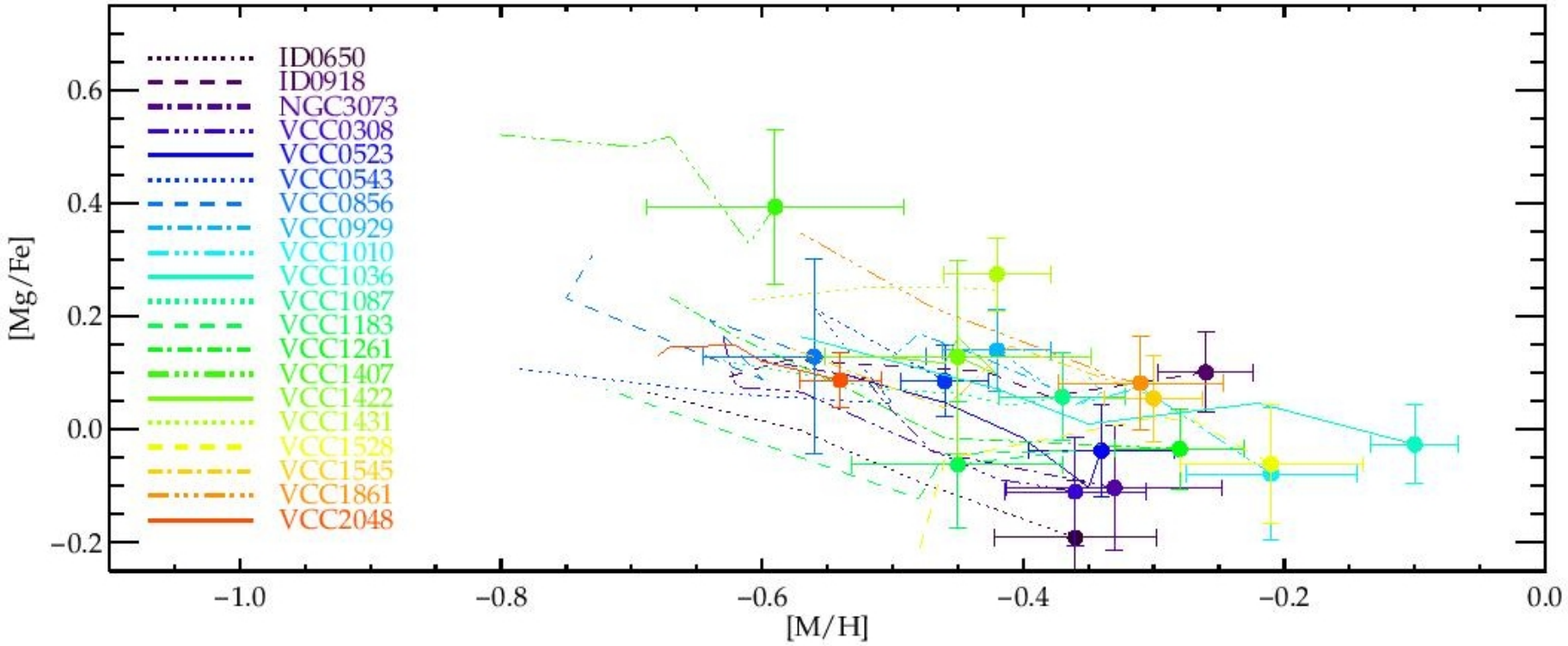

Figure 1. [Mg/Fe] abundance ratio as a function of [M/H] of the 20 low-mass early-type galaxies of S17 from the Virgo cluster and the field/group environment. The galaxy centers have been marked with filled circles, error bars are shown for central points (the outermost profile points have error bars typically ∼twice as large as the central ones – for the full profiles with uncertainties see the appendix of the above paper).

Разбивка по локальным дисперсиям скоростей

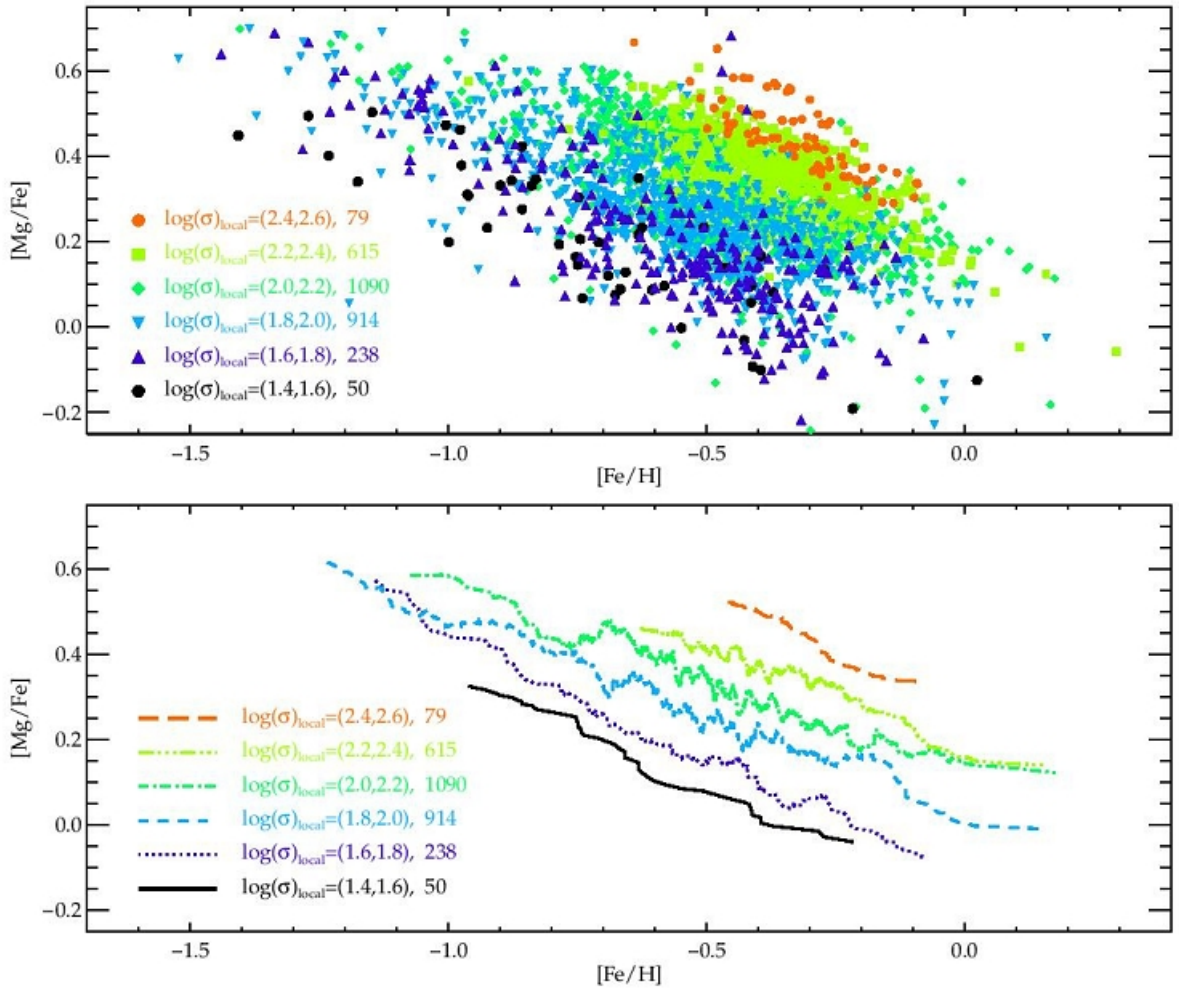

Figure 2. **Upper panel:** [Mg/Fe] abundance ratio as a function of [Fe/H] for all the profile points from the S17 sample as well as ATLAS^{3D} galaxies, color-coded by σ_{local} values as explained in the legend, with the number of points falling into each bin provided next to the bin ranges. **Lower panel:** running averages of all the profile points for the above defined σ bins (same color-coding). [Fe/H] values have been obtained from [M/H] using the formula of Vazdekis et al. (2015): $[Fe/H] = [M/H] - 0.75 \cdot [Mg/Fe]$. Note that the running averages are *not* averaged profiles as they combine points based on their

Параллельный ход с тонким диском нашей Галактики?